Research Article | Vol. 11, No. 1 / 1 January 2020 / Biomedical Optics Express 406
Biomedical Optics EXPRESS

Identifying different types of microorganisms with terahertz spectroscopy

S. A. Yoon,[1,3] S. H. Cha,[1,3] S. W. Jun,[1] S. J. Park,[1] J.-Y. Park,[1] S. Lee,[1] H. S. Kim,[2] and Y. H. Ahn[1,*]

[1]Department of Physics and Department of Energy Systems Research, Ajou University, Suwon 16499, South Korea
[2]Department of Biological Science, Ajou University, Suwon 16499, South Korea
[3]Co-first authors with equal contribution
[*]ahny@ajou.ac.kr

Abstract: Most microbial detection techniques require pretreatment, such as fluorescent labeling and cultivation processes. Here, we propose novel tools for classifying and identifying microorganisms such as molds, yeasts, and bacteria based on their intrinsic dielectric constants in the THz frequency range. We first measured the dielectric constant of films that consisted of a wide range of microbial species, and extracted the values for the individual microbes using the effective medium theory. The dielectric constant of the molds was 1.24–1.85, which was lower than that of bacteria ranging from 2.75–4.11. The yeasts exhibited particularly high dielectric constants reaching 5.63–5.97, which were even higher than that of water. These values were consistent with the results of low-density measurements in an aqueous environment using microfluidic metamaterials. In particular, a blue shift in the metamaterial resonance occurred for molds and bacteria, whereas the molds have higher contrast relative to bacteria in the aqueous environment. By contrast, the deposition of the yeasts induced a red shift because their dielectric constant was higher than that of water. Finally, we measured the dielectric constants of peptidoglycan and polysaccharides such as chitin, α-glucan, and β-glucans (with short and long branches), and confirmed that cell wall composition was the main cause of the observed differences in dielectric constants for different types of microorganisms.

1. Introduction

Rapid and accurate identification of hazardous microorganisms (or pathogens) is essential for the effective treatment of deadly diseases, such as sepsis, and the prevention of further infections [1]. However, contemporary microbial detection tools are limited by low detection speed, which usually extends over a couple of days. In general, culture-based detection methods, including polymerase chain reaction (PCR) systems, have been widely used to detect and quantify microorganisms [2–4]. Although PCR is capable of detecting a wide range of infectious fungi and bacteria, this method is generally time-consuming and labor-intensive. In many cases, it is crucial to classify the types of pathogens as early as possible before the individual species are distinguished. Therefore, it is essential to develop diagnosis tools with which we can exploit the inherent physical properties of the microorganisms without necessitating pretreatment procedures such as fluorescent labeling and cell cultivation.

One powerful approach for the identification and classification of microorganisms is optical and electron microscope imaging of their morphology and intracellular organelles [5,6]. On the other hand, gene amplification and sequencing of DNA and RNA have been adopted as important tools for classifying a broad range of bacteria and fungi targets. For instance, in the late 1970s, a three-domain system introduced by Woese et al. divided cellular life forms into archaea, bacteria, and eukaryotes (which include fungi) on the basis of ribosomal RNA analysis [7,8]. Importantly, because cell walls are unique with respect to different types of microorganisms,

#376584 https://doi.org/10.1364/BOE.376584
Journal © 2020 Received 29 Aug 2019; revised 10 Dec 2019; accepted 11 Dec 2019; published 23 Dec 2019

Biomedical Optics EXPRESS

their structure and composition could work as an excellent target for the development of novel selective identification tools [9–11]. For instance, in the case of bacteria, Gram staining methods have been widely adopted to distinguish and classify bacterial species into two large groups (Gram-positive and Gram-negative) based on the chemical and physical properties of their cell walls [12,13]. However, Gram staining requires a labeling process, and distinction in terms of cell wall composition has been largely unexplored for other types of microorganisms, such as molds and yeasts.

Recently, THz metamaterials have emerged as real-time and sensitive tools for the detection of living and viable microorganisms [14–16]. Because the metamaterial sensing is dielectric sensing, obtaining information on the dielectric constant of the target substances is the primary step for the practical application of the sensors [17–23]. Label-free detection has been introduced using functionalized devices, for instance, by coating the substrate with the antibody specific to the analytes [24,25]. However, the use of antibody is costly and does not persist in general, thereby making the sensors disposable. Therefore, a novel approach for differentiating the types of microbes in terms of their intrinsic properties, such as the dielectric constant, will provide a breakthrough in the development of an early identification tool.

In this work, we performed THz time-domain spectroscopy on representative microorganisms ranging from molds, yeasts, and bacteria, and found that it was possible to classify them in terms of their dielectric constant. We first extracted the dielectric constant of the microbial films, from which we then obtained the indexes for the individual species using the effective medium theory. Their dielectric constants were consistent with results of a study performed in an aqueous environment that exploited the metamaterial sensors incorporated into the fluidic channels. Finally, we revealed that the differences in cellular structures, especially in cell wall compositions, were responsible for the different dielectric constants among the different types of microorganisms.

2. Methods

2.1. Preparation of microorganism samples

We prepared representative microorganisms including molds, bacteria, and yeasts. They were grown by a streaking on medium method followed by incubation for 2 d, obtained initially either from the Korean Agricultural Culture Collection (KACC) or the Korean Collection for Type Cultures (KCTC). The culture media and the incubation temperature varied from sample to sample as follows: *Penicillium chrysogenum* (PC; KACC 45971; malt extract agar; 25 °C), *Aspergillus niger* (AN; KACC 40280; malt extract agar; 25 °C), *Monascus pilosus* (MP; KCTC 42430; malt extract agar; 25 °C), *Rhizopus oryzae* (RO; KCTC 6944; potato dextrose agar; 24 °C), *Mucor ambiguous* (MA; KCTC 26787; malt extract agar; 25 °C), and *Trichoderma viride* (TV; KACC 44532; malt extract agar; 20 °C) for molds; *Escherichia coli* (EC; KACC 11598; nutrient agar; 37 °C), *Alcaligenes faecalis* (AF; KCTC 2678; nutrient agar; 37 °C), *Pseudomonas aeruginosa* (PA; KCTC 1750; nutrient agar; 37 °C), *Lactobacillus casei* (LC; KCTC 13086; MRS agar; 37 °C), *Bacillus subtilis* (BS; KCTC 3725; malt extract agar; 30 °C), and *Staphylococcus aureus* (SA; KCTC 1928; nutrient agar; 37 °C) for bacteria; and *Saccharomyces cerevisiae* (SC; KCTC 27139; glucose-peptone-yeast extract agar; 25 °C) and *Schizosaccharomyces pombe* (SP; KCTC 27259; glucose-peptone-yeast extract agar; 25 °C) for yeasts. Their microscopic images and general characteristics such as size and shape can be found in the references included in Table 1. For the dielectric constant measurements on the microbial films, we prepared thick and dense films by stacking the large amount of fungi and bacteria layer by layer on a cellulose membrane until they reach the thickness of 200–600 μm.

Biomedical Optics EXPRESS

2.2. Preparation of polysaccharide films

To measure the THz dielectric constants of the polysaccharide films, we fabricated a thick and dense pallet from powders purchased from Sigma-Aldrich, such as peptidoglycan (extracted from BS, Sigma no. 69554), chitin (from shrimp shells, Sigma no. C 7170), β-glucan with short branches (from *Laminaria digitata*, Sigma no. L 9634), and β-glucan with long branches (from SC, Sigma no. G 5011). We required additional processes to prepare the glucan pallets with triple strand structures [26]. Both β-glucan (LB and SB) samples were isolated using an alkaline-acid hydrolysis method to form the triple helix structure, followed by freeze-drying for 12 h. Conversely, α-glucan was isolated from starch solutions using a phase separation method followed by freeze-drying for 12 h [27].

2.3. Fabrication of fluidic devices with metamaterial patterns

Metamaterial patterns were prepared using a conventional photolithography method on a high-resistivity Si substrate (resistivity > 6000 Ω·cm, and thickness of 550 μm). Cr (2 nm) and Au (98 nm) metal films were deposited using an e-beam evaporator in order to define the arrays of split-ring resonator patterns with a linewidth of 4 μm, outer dimensions of 36 μm × 36 μm, and gap size of 3 μm. The fluidic channel, with a height of 20 μm and width of 2 mm, was prepared by pouring Polydimethylsiloxane (PDMS) onto a SU-8 mold used to form a trench structure in PDMS. It was bonded to the substrate containing the metamaterial patterns after plasma surface treatment [28]. The microbial solution was injected into the fluidic channel using a syringe pump.

2.4. THz time-domain spectroscopy

The real-time THz transmission amplitudes of the metamaterials with fungi were measured with a conventional THz time-domain spectroscopy (THz-TDS) setup, as found in our previous studies [14–16]. Briefly, a femtosecond laser at $\lambda = 800$ nm was incident on the photoconductive antenna, which emitted a linearly polarized THz pulse. Subsequently, this THz pulse was focused on the microbial films and the metamaterials with an approximately 1 mm spot diameter under ambient conditions. Time traces of the transmitted THz electric field both in amplitude and phase were measured by varying the time delay between the 800 nm probe beam and the THz pulse. The THz spectrum was taken by applying a fast Fourier transform to the time trace, and was normalized with respect to the reference.

3. THz dielectric constant of different types of microorganisms

We investigated the dielectric properties of representative molds, yeasts, and bacteria, extending the fundamental knowledge of microorganisms with a unifying perspective. This is based on the expectation that the dielectric properties of each group of microorganisms would be different because they have different cellular structures as summarized in Fig. 1(a). In particular, the cell wall composition plays an important role in the case of molds and yeasts because they have relatively thick walls that consist of various kinds of polysaccharides as will be discussed in detail later [10,29,30]. Conversely, water comprises most of bacterial wall with a relatively thin wall consisting of peptidoglycan [31].

We first measured the complex dielectric constants of the molds, yeasts, and bacteria by preparing thick and dense microbial films with a thickness of 200–600 μm. By measuring both the amplitudes and phases of the transmitted THz pulses through the thick microbial films, we extracted the complex dielectric constants of the films that consisted of closely packed fungi and bacteria. The representative dielectric constants ($\varepsilon_{\text{film}}$) of the microbial films are shown in Fig. 1(b) for the three different species selected from the molds (*Aspergillus niger*), yeasts (*Saccharomyces cerevisiae*), and bacteria (*Escherichia coli*). The real part of the dielectric constant of the bacterial film reached approximately 2, whereas that of mold showed a value

Biomedical Optics EXPRESS

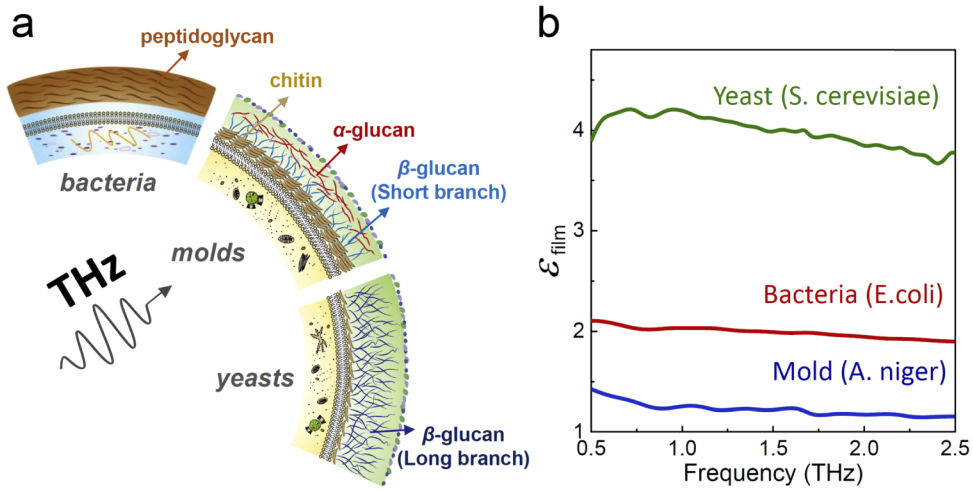

Fig. 1. (a) Schematic images of cell wall structures for molds, yeasts, and bacteria, including their compositions. (b) Plots of frequency-dependent dielectric constants of representative microbial films of yeast (S. cerevisiae), bacteria (E. coli), and mold (A. niger).

very close to 1 over a wide frequency range from 0.5–2.5 THz. In particular, the dielectric constant of the yeast was very high, and reached approximately 4.2 at 1 THz. By comparison, the imaginary components were negligible in the case of mold films indicating that they are mostly transparent in the THz frequency range, whereas the bacterial films (0.21–0.37) and the yeast films (0.32–0.55) exhibited relatively high imaginary values.

We extended our measurements into a variety of microbial films (out of 14 species) ranging from molds, yeasts, and bacteria, and the results are summarized in Fig. 2(a). In other words, the dielectric constant ranged 1.15–1.62 for mold films and 2.03–2.70 for bacterial films, while those of yeasts exhibited very high values of 4.17–4.38. Evidently, these results reveal that the microorganisms can be classified based on their intrinsic properties (i.e., dielectric properties) without necessitating the fluorescent labeling and genetic sequencing. We excluded data for molds (such as *Neurospora intermedia* with an $\varepsilon_{\text{film}}$ of approximately 1.69) that were covered by hyphae and showed relatively higher values than those shown in Fig. 2(a) (but still lower than those of bacteria).

The dielectric constants of the individual fungi and bacteria could be obtained from those of the films by using the effective medium theory (Bruggeman model) of $(\varepsilon_{\text{film}} - 1)/3\varepsilon_{\text{film}} = f(\varepsilon_{\text{f}} - 1)/(\varepsilon_{\text{f}} + 2\varepsilon_{\text{film}})$, where f is the packing fraction of the fungi and bacteria contained in the films [32]. In order to obtain the dielectric constants, we extracted the volume fraction of the individual fungi and bacteria that comprised the microbial films from the shape of the individual microorganisms as summarized in Table 1. In general, the packing fraction depends strongly on the aspect ratio because it influences the arrangement in the closely packed layers for the rod and ellipsoid shapes. The explicit relation between the aspect ratio and the packing fraction has been reported in the Refs. [33–35]; conversely, we assumed the closely packed lattice with $f = 0.64$ in the case of spherical shape. For instance, the volume fraction $f = 0.74$–0.80 was chosen for SC (yeast) having an ellipsoid shape with an aspect ratio of 1.25–1.50, and $f = 0.62$–0.67 was chosen for LC (bacteria) having a rod shape with an aspect ratio of 2.5–3.6. As a result, the real part of the dielectric constant ε_{r} was measured as 5.63 and 2.84 (in terms of median value) for SC and LC, respectively.

The complex dielectric constants of the individual microorganisms extracted from the effective medium theory are summarized in Fig. 2(b) for the three different types of microorganisms.

Biomedical Optics EXPRESS

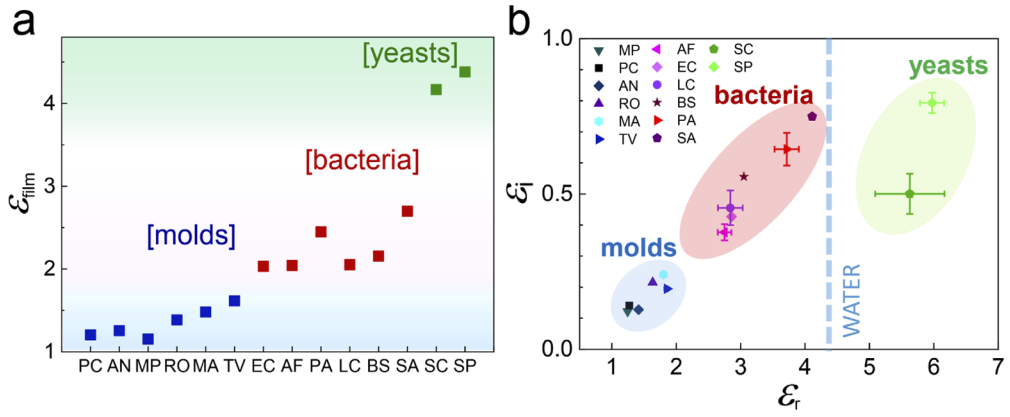

Fig. 2. (a) Real part of dielectric constants at 1 THz for three different types of microbial films, including molds (6 species), bacteria (6 species), and yeasts (2 species). (b) Plot of complex dielectric constants of individual microorganisms extracted using the effective medium theory.

Table 1. Size, shape, aspect ratio (α), and the fractional coefficient (f) for the microbial species in Fig. 2.

Species	Size (μm)	Shape	ε_{film}	α	f	ε_r	ε_i	Ref.
Molds								
P. chrysogenum	2.5 × 4.0	ellipsoid	1.20	1.6	0.76	1.27	0.14	[37]
A. niger	3.5–4.7	sphere	1.26	1	0.64	1.41	0.13	[38]
M. pilosus	5.0	sphere	1.15	1	0.64	1.24	0.12	[39]
R. oryzae	4.0–10.0	sphere	1.38	1	0.64	1.63	0.22	[40]
M. ambiguus	4.0–6.0	sphere	1.45	1	0.64	1.80	0.24	[41]
T. viride	(1.0–2.5) × (1.5–4.0)	ellipsoid	1.62	1.5–1.6	0.75–0.76	1.85	0.19	[42]
Bacteria								
E. coli	1.0 × 3.0	rod	2.03	3	0.63	2.86	0.43	[43]
A. faecalis	(0.4) × (0.7–1.0)	rod	2.04	1.75–2.5	0.65–0.68	2.75	0.38	[44]
P. aeruginosa	(0.5–0.8) × (1.5–3.0)	rod	2.45	3–3.75	0.61–0.64	3.72	0.64	[45]
L. casei	(0.6–1.1) ×(1.5–4.0)	rod	2.05	2.5–3.64	0.62–0.67	2.84	0.46	[46]
B. subtilis	1.0 × 2.8	rod	2.16	2.8	0.64	3.05	0.56	[47]
S. aureus	1.5	sphere	2.70	1	0.64	4.11	0.75	[48]
Yeasts								
S. cerevisiae	4.0 × (5.0–6.0)	ellipsoid	4.17	1.25–1.5	0.74–0.8	5.63	0.50	[49]
S. pombe	4.0 × (9.1–9.9)	ellipsoid	4.38	2.27 –2.47	0.78–0.8	5.97	0.79	[50]

Biomedical Optics EXPRESS

Focusing on the real part of the dielectric constant, it ranged 1.24–1.85 for molds and 2.75–4.11 for bacteria. Again, they were well classified with respect to the dielectric constant values, while they were less than that of water (ε_r of approximately 4.3) [36]. Importantly, in the case of the yeasts, it reached as high as 5.63–5.97, which was even higher than the water values. The origin of the distinct identification of different microbial groups will be revealed later with respect to their cell compositions. Until now, current identification of microorganisms primarily depends on the observation of their morphology and sequencing of genetic materials, and their classification in terms of their dielectric constant has never been demonstrated before. Importantly, our work will allow us to identify the types of microorganisms in the early stage based on their intrinsic properties without procedures such as fluorescent labeling and cultivation.

4. Low-density sensing in aqueous environment

Next, we demonstrate the results of sensing low-density microorganisms using metamaterial sensors in an aqueous environment, which exhibited results consistent with the dielectric constant values obtained above. We incorporated the metamaterial pattern into the fluidic devices and monitored the change in the resonant frequency upon the flow of the liquid solution containing the different species of microorganisms, as schematically illustrated in Fig. 3(a). THz transmission spectra were obtained using THz time-domain spectroscopic techniques with an acquisition time of 5 s for each spectrum [14–16]. The metamaterial resonance was determined by the LC resonance, i.e., with $f_0 = 1/(2\pi\sqrt{LC})$ [18]. The dielectric microorganisms placed in the gap area would cause a change in the effective dielectric constants of the capacitor, thereby resulting in a shift of the resonant frequency in metamaterials. The frequency shift Δf can be expressed as $\Delta f/f_0 \propto -(\varepsilon_{\text{microbe}} - \varepsilon_{\text{water}})/\varepsilon_{\text{eff}}$, where $\varepsilon_{\text{microbe}}$ is the dielectric constant of the deposited microorganisms, $\varepsilon_{\text{water}}$ is that of water, ε_{eff} is the effective dielectric constant without the deposition of fungi.

The frequency shift was monitored as a function of the volume density of the microbial solutions. The representative spectra are shown in Fig. 3(b) for two different species of microorganisms from the yeasts (SC) and molds (AN) before and after the injection of the low-density solution into the channel. Without the surface functionalization procedures, we waited for 20 min every time after we injected the solutions so that a considerable amount of species could be precipitated at the surface of the metamaterials. First, clear blue shifts ($\Delta f > 0$) were observed in the case of the molds. This was because the dielectric constant of molds was smaller than that of water (i.e., $\varepsilon_{\text{microbe}} < \varepsilon_{\text{water}}$); hence, a reduction in the effective dielectric constant will occur as microbes occupy part of the gap area. By contrast, in the case of the yeasts, a red shift was observed ($\Delta f < 0$), which could have been due to the fact that the dielectric constant of the yeasts was higher than that of water (i.e., $\varepsilon_{\text{microbe}} > \varepsilon_{\text{water}}$), as shown in Fig. 2(b).

The frequency shift is plotted as a function of the solution density in Fig. 3(c) for the 11 different microbes (4 molds, 6 bacteria, and 1 yeast). The solution density was estimated using light-scattering methods in reference to that of *Penicillium*, which was evaluated by cell counting methods using an optical microscope. We found that the frequency shifts of the molds were much higher than those of bacteria for all the species we tested, although they all exhibited blue shifts. This was consistent with the fact that the mold indexes had a higher contrast with respect to the water values than those of bacteria, as shown in Fig. 2(b). In other words, the bacteria were more sensitive in ambient conditions, whereas the molds were more sensitive in the aqueous phase.

On the other hand, yeasts exhibited a frequency shift in the opposite direction because they had a higher dielectric constant relative to that of water as mentioned above. Overall, these results illustrated that although the dielectric constant values shown in Fig. 2 were measured in a dried condition, they are also applicable in aqueous environments. Although the fluidic experiments were performed with the metamaterial resonance at around 0.8 THz, the dielectric constant of the microbes obtained at 1 THz is still applicable because it is uniform over the wide spectral

Biomedical Optics EXPRESS

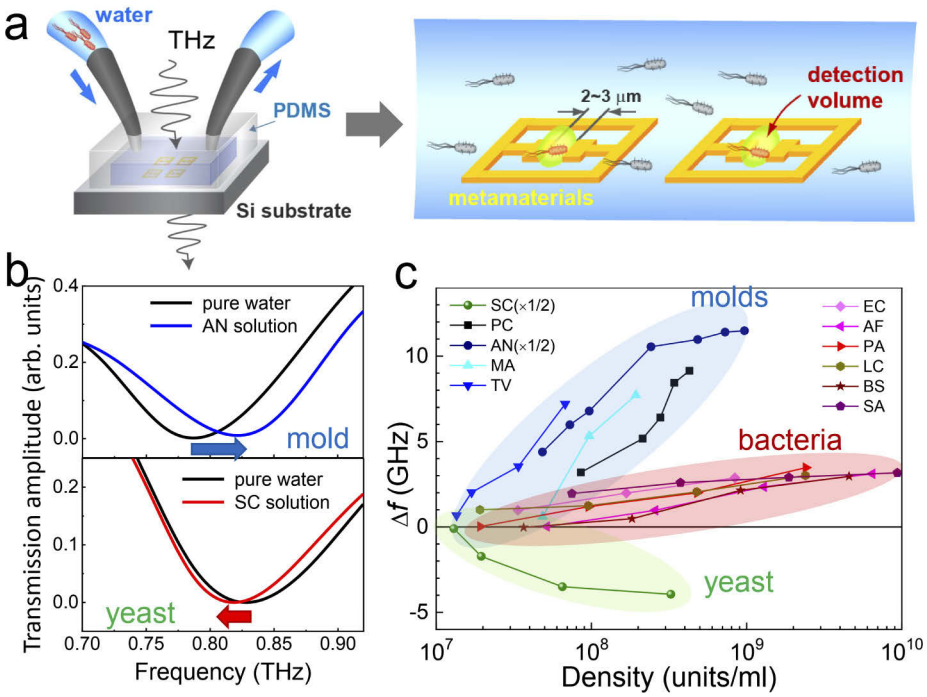

Fig. 3. (a) A schematic presentation of THz metamaterials sensing of liquids containing low-density microorganisms. (b) The resonance shifts of THz metamaterials measured for low-density mold (top) and yeast (bottom) solutions with densities of 2.4×10^8 and 8×10^7 units/ml, respectively. (c) Plot of frequency shift as a function of number density for different species.

range as shown in Fig. 1(b). We note that the accurate identification of individual species was limited in the current study, because many portion of the microbes are located outside of the detection volume (which is highly localized around the gap area), as schematically shown in Fig. 3(a). This necessitates future investigation into developing advanced sensors with which we can capture the microbes exclusively around the gap structures as early as possible, and also into designing novel sensors with enhanced sensitivity for single cell identification.

5. Dielectric properties of cell wall compositions

The origin of the distinct identification of different groups of microbes can be understood in the context of differences in their cell structure. The cell wall of molds consists of α-glucan, chitin, and β-glucan, as schematically illustrated in Fig. 4(a), although their relative fraction differs significantly with different species [10]. Conversely, the composition of yeast is generally dominated by β-glucan [29,30]. We noted that chitin has a linear chain structure and that α-glucan has a single-stranded helix (SSH) structure [51–54]. Significantly, (1,3) β-glucan has a triple-stranded helix (TSH) structure with (1,6) linked branches. It has been reported that β-glucan found in molds has short branches (SB), whereas it has long branches (LB) with large molecular weight in yeast cells [55–59].

We prepared various polysaccharide films as described in the methods section, and their dielectric constants at 1 THz are illustrated in Fig. 4(b). Focusing on the mold and yeast walls, the indexes for the chitin (linear chain) and α-glucan (SSH) were measured as 1.60 and 1.98, respectively, at 1 THz. Many kinds of molds have relatively large compositions of chitin and

Biomedical Optics EXPRESS

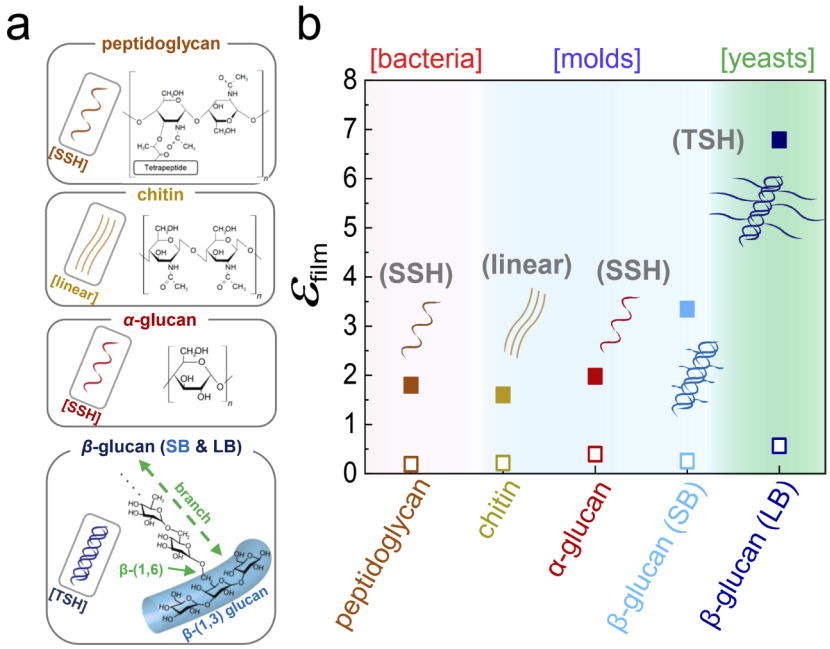

Fig. 4. (a) Schematic images of molecular structures for peptidoglycan, chitin, α-glucan, and β-glucans. (b) Real (filled boxes) and imaginary (open boxes) parts of dielectric constants for peptidoglycan and polysaccharides films, measured at 1 THz.

α-glucan, which is consistent with the dielectric constant values shown in Fig. 2. Significantly, β-glucan, which has a TSH structure, had a very large value compared with those of chitin and α-glucan. Furthermore, we found that β-glucan with LB had extremely large indexes of 6.79 at 1 THz compared with that of the SB (3.34 at 1 THz). Therefore, the yeast index, which had large values of 5.63–5.97, could be understood by the large composition of (1,3) β-glucan (TSH structure) with LB.

On the other hand, bacterial cell wall thickness ranged from 20–80 nm, which was thinner than that of fungi. The dielectric constant of the peptidoglycan with a SSH structure, which is the main composition of the bacterial wall, was measured to be 1.8 at 1 THz as shown in Fig. 4(b). Importantly, water comprises most of the mass of bacteria in general as mentioned before [31]; therefore, the dielectric constant of the bacteria could be described by the simple model of a rod-shaped water capsule surrounded by the dielectric shell. This is also consistent with the observation of the relatively large imaginary components of bacteria as shown in Fig. 2(b).

The results in Fig. 4 suggest that there should be a strong correlation between the dielectric constant of cell wall compositions and their molecular structure. This is a very interesting issue, necessitating future investigation based on an elaborate theoretical analysis. In particular, the exceptionally high index for the long-branched β-glucan is likely due to large polarizability of the branch structure, in which case the dielectric index could be tuned by engineering the branch structures. We note that the polysaccharide films such as β-glucan could be useful for fabricating optical devices in which the large index is required in the THz frequency range. Clearly, information on the dielectric constant of microorganisms in conjunction with their cellular composition will be crucial for various applications with functional biomaterials, as well as for their early identification.

Biomedical Optics EXPRESS

6. Conclusion

To conclude, we proposed novel classification and identification tools for microorganisms, including molds, yeasts, and bacteria, based on their intrinsic dielectric constants in the THz frequency range. We first measured the dielectric constants of the various species of microorganisms, from which we extracted the values for the individual microbes. The indexes of the molds ranged from 1.24–1.85, but these were higher in the case of bacteria ranging from 2.75–4.11, which were relatively close to the values for water. The yeasts showed a particularly high dielectric constant reaching 5.63–5.97, which was even higher than that of water. These values were consistent with the results of low-density measurements in an aqueous environment using microfluidic metamaterials. In particular, a blue shift in the metamaterial resonance occurred for molds and bacteria, whereas the molds were more sensitive than bacteria. By contrast, the deposition of yeasts induced a red shift because their dielectric constant was higher than that of water. Finally, we measured the dielectric constants of peptidoglycan and polysaccharides such as chitin, α-glucan, and β-glucans (with SB and LB), thereby confirming that cell wall composition was the main cause of the observed differences in dielectric constants for different types of microorganisms. Our approach is likely to constitute an important breakthrough for a novel classification tool for various living organisms and for the fabrication of highly sensitive biosensors, thereby enabling high-speed, label-free detection of pathogens in various environments.

Funding

National Research Foundation of Korea (2017R1A2B4009177); Korea Institute of Energy Technology Evaluation and Planning (20184030202220).

Acknowledgments

This work was supported by the Midcareer Researcher Program (2017R1A2B4009177) through a National Research Foundation grant funded by the Korea Government and by the Human Resources Program in Energy Technology (20184030202220) of the Korea Institute of Energy Technology Evaluation and Planning (KETEP) grant funded by the Korea Government.

Disclosures

The authors declare that there are no conflicts of interest related to this article.

References

1. S. M. Yoo and S. Y. Lee, "Optical Biosensors for the Detection of Pathogenic Microorganisms," Trends Biotechnol. **34**(1), 7–25 (2016).
2. K. Makimura, S. Y. Murayama, and H. Yamaguchi, "Detection of a wide range of medically important fungi by the polymerase chain reaction," J. Med. Microbiol. **40**(5), 358–364 (1994).
3. P. Belgrader, W. Benett, D. Hadley, J. Richards, P. Stratton, R. Mariella, and F. Milanovich, "PCR detection of bacteria in seven minutes," Science **284**(5413), 449–450 (1999).
4. A. Niemz, T. M. Ferguson, and D. S. Boyle, "Point-of-care nucleic acid testing for infectious diseases," Trends Biotechnol. **29**(5), 240–250 (2011).
5. G. A. Bartlett, "Scanning electron microscope: potentials in the morphology of microorganisms," Science **158**(3806), 1318–1319 (1967).
6. J. Porter, "Antony van Leeuwenhoek: tercentenary of his discovery of bacteria," Microbiol. Mol. Biol. Rev. **40**, 260 (1976).
7. C. R. Woese and G. E. Fox, "Phylogenetic structure of the prokaryotic domain: the primary kingdoms," Proc. Natl. Acad. Sci. U. S. A. **74**(11), 5088–5090 (1977).
8. C. R. Woese, O. Kandler, and M. L. Wheelis, "Towards a natural system of organisms: proposal for the domains Archaea, Bacteria, and Eucarya," Proc. Natl. Acad. Sci. U. S. A. **87**(12), 4576–4579 (1990).
9. M. C. Maiden, J. A. Bygraves, E. Feil, G. Morelli, J. E. Russell, R. Urwin, Q. Zhang, J. Zhou, K. Zurth, and D. A. Caugant, "Multilocus sequence typing: a portable approach to the identification of clones within populations of pathogenic microorganisms," Proc. Natl. Acad. Sci. U. S. A. **95**(6), 3140–3145 (1998).

Biomedical Optics EXPRESS

10. S. M. Bowman and S. J. Free, "The structure and synthesis of the fungal cell wall," BioEssays **28**(8), 799–808 (2006).
11. D.-J. Scheffers and M. G. Pinho, "Bacterial cell wall synthesis: new insights from localization studies," Microbiol. Mol. Biol. Rev. **69**(4), 585–607 (2005).
12. J. W. Bartholomew and T. Mittwer, "The gram stain," Microbiol. Mol. Biol. Rev. **16**, 1 (1952).
13. T. J. Beveridge, "Use of the Gram stain in microbiology," Biotech. Histochem. **76**(3), 111–118 (2001).
14. S. J. Park, J. T. Hong, S. J. Choi, H. S. Kim, W. K. Park, S. T. Han, J. Y. Park, S. Lee, D. S. Kim, and Y. H. Ahn, "Detection of microorganisms using terahertz metamaterials," Sci. Rep. **4**, 4988 (2015).
15. S. J. Park, B. H. Son, S. J. Choi, H. S. Kim, and Y. H. Ahn, "Sensitive detection of yeast using terahertz slot antennas," Opt. Express **22**(25), 30467–30472 (2014).
16. S. J. Park, S. H. Cha, G. A. Shin, and Y. H. Ahn, "Sensing viruses using terahertz nano-gap metamaterials," Biomed. Opt. Express **8**(8), 3551–3558 (2017).
17. H.-T. Chen, W. J. Padilla, J. M. Zide, A. C. Gossard, A. J. Taylor, and R. D. Averitt, "Active terahertz metamaterial devices," Nature **444**(7119), 597–600 (2006).
18. H.-T. Chen, W. J. Padilla, R. D. Averitt, A. C. Gossard, C. Highstrete, M. Lee, J. F. O'Hara, and A. J. Taylor, "Electromagnetic metamaterials for terahertz applications," IEEE Trans. Terahertz Sci. Technol. **1**(1), 42–50 (2008).
19. H. Tao, L. R. Chieffo, M. A. Brenckle, S. M. Siebert, M. Liu, A. C. Strikwerda, K. Fan, D. L. Kaplan, X. Zhang, R. D. Averitt, and F. G. Omenetto, "Metamaterials on paper as a sensing platform," Adv. Mater. **23**(28), 3197–3201 (2011).
20. J. F. O'Hara, W. Withayachumnankul, and I. Al-Naib, "A review on thin-film sensing with terahertz waves," J. Infrared Millim. Terahertz Waves **33**(3), 245–291 (2012).
21. H. Tao, M. A. Brenckle, M. Yang, J. Zhang, M. Liu, S. M. Siebert, R. D. Averitt, M. S. Mannoor, M. C. McAlpine, and J. A. Rogers, "Silk-based conformal, adhesive, edible food sensors," Adv. Mater. **24**(8), 1067–1072 (2012).
22. J. F. O'Hara, R. Singh, I. Brener, E. Smirnova, J. Han, A. J. Taylor, and W. Zhang, "Thin-film sensing with planar terahertz metamaterials: sensitivity and limitations," Opt. Express **16**(3), 1786–1795 (2008).
23. A. K. Azad, J. Dai, and W. Zhang, "Transmission properties of terahertz pulses through subwavelength double split-ring resonators," Opt. Lett. **31**(5), 634–636 (2006).
24. A. Menikh, S. P. Mickan, H. Liu, R. MacColl, and X.-C. Zhang, "Label-free amplified bioaffinity detection using terahertz wave technology," Biosens. Bioelectron. **20**(3), 658–662 (2004).
25. X. Wu, B. Quan, X. Pan, X. Xu, X. Lu, C. Gu, and L. Wang, "Alkanethiol-functionalized terahertz metamaterial as label-free, highly-sensitive and specific biosensor," Biosens. Bioelectron. **42**, 626–631 (2013).
26. H. J. Shin, S. J. Oh, S. I. Kim, H. Won Kim, and J.-H. Son, "Conformational characteristics of β-glucan in laminarin probed by terahertz spectroscopy," Appl. Phys. Lett. **94**(11), 111911 (2009).
27. S. Kim and J. L. Willett, "Isolation of amylose from starch solutions by phase separation," Starch/Staerke **56**(1), 29–36 (2004).
28. S. J. Park, S. A. N. Yoon, and Y. H. Ahn, "Dielectric constant measurements of thin films and liquids using terahertz metamaterials," RSC Adv. **6**(73), 69381–69386 (2016).
29. F. M. Klis, "Cell wall assembly in yeast," Yeast **10**(7), 851–869 (1994).
30. F. M. Klis, P. Mol, K. Hellingwerf, and S. Brul, "Dynamics of cell wall structure in Saccharomyces cerevisiae," FEMS Microbiol. Rev. **26**(3), 239–256 (2002).
31. M. Potts, "Desiccation tolerance of prokaryotes," Microbiol. Rev. **58**, 755–805 (1994).
32. M. Scheller, C. Jansen, and M. Koch, "Applications of effective medium theories in the terahertz regime," in *Recent Optical and Photonic Technologies* (InTech, 2010).
33. A. Donev, F. H. Stillinger, P. Chaikin, and S. Torquato, "Unusually dense crystal packings of ellipsoids," Phys. Rev. Lett. **92**(25), 255506 (2004).
34. P. Chaikin, A. Donev, W. Man, F. H. Stillinger, and S. Torquato, "Some observations on the random packing of hard ellipsoids," Ind. Eng. Chem. Res. **45**(21), 6960–6965 (2006).
35. A. Wouterse, S. R. Williams, and A. P. Philipse, "Effect of particle shape on the density and microstructure of random packings," J. Phys.: Condens. Matter **19**(40), 406215 (2007).
36. C. Rønne, L. Thrane, P. O. Åstrand, A. Wallqvist, K. V. Mikkelsen, and S. R. Keiding, "Investigation of the temperature dependence of dielectric relaxation in liquid water by THz reflection spectroscopy and molecular dynamics simulation," J. Chem. Phys. **107**(14), 5319–5331 (1997).
37. A. H. Fouda, S. E.-D. Hassan, A. M. Eid, and E. E.-D. Ewais, "Biotechnological applications of fungal endophytes associated with medicinal plant Asclepias sinaica (Bioss.)," Ann. Agric. Sci. **60**(1), 95–104 (2015).
38. T. Tsukahara, M. Yamada, and T. Itagaki, "Micromorphology of conidiospores of Aspergillus niger by electron microscopy," Jpn. J. Microbiol. **10**(2), 93–107 (1966).
39. A. Pordel, A. Ahmadpour, M. Behnia, and M. Javan-Nikkhah, "New records of Hyphomycetes fungi in Iran," Mycologia Iranica **2**, 69–74 (2015).
40. J.-H. Kwon, J. Kim, and W.-I. Kim, "First report of Rhizopus oryzae as a postharvest pathogen of apple in Korea," Mycobiology **39**(2), 140–142 (2011).
41. P. C. Iwen, L. Sigler, R. K. Noel, and A. G. Freifeld, "Mucor circinelloides was identified by molecular methods as a cause of primary cutaneous zygomycosis," J. Clin. Microbiol. **45**(2), 636–640 (2007).
42. I.-Y. Choi, S.-B. Hong, and M. C. Yadav, "Molecular and morphological characterization of green mold, Trichoderma spp. isolated from oyster mushrooms," Mycobiology **31**(2), 74–80 (2003).

Biomedical Optics EXPRESS

43. G. Reshes, S. Vanounou, I. Fishov, and M. Feingold, "Cell shape dynamics in Escherichia coli," Biophys. J. **94**(1), 251–264 (2008).
44. S. Ju, J. Lin, J. Zheng, S. Wang, H. Zhou, and M. Sun, "Alcaligenes faecalis ZD02 is a novel nematicidal bacterium, with an extracellular serine protease (Esp) as a virulence factor," Appl. Environ. Microbiol., AEM., **2016**, 03444–03415 (2016).
45. S. Chattopadhyay, S. D. Perkins, M. Shaw, and T. L. Nichols, "Evaluation of exposure to Brevundimonas diminuta and Pseudomonas aeruginosa during showering," J. Aerosol Sci. **114**, 77–93 (2017).
46. G. Nagy, G. Pinczes, G. Pinter, I. Pocsi, J. Prokisch, and G. Banfalvi, "In situ electron microscopy of lactomicroselenium particles in probiotic bacteria," Int. J. Mol. Sci. **17**, 1047 (2016).
47. O. Sahin, E. H. Yong, A. Driks, and L. Mahadevan, "Physical basis for the adaptive flexibility of Bacillus spore coats," J. Royal Soc. Interface **9**(76), 3156–3160 (2012).
48. J. M. Monteiro, P. B. Fernandes, F. Vaz, A. R. Pereira, A. C. Tavares, M. T. Ferreira, P. M. Pereira, H. Veiga, E. Kuru, and M. S. VanNieuwenhze, "Cell shape dynamics during the staphylococcal cell cycle," Nat. Commun. **6**(1), 8055 (2015).
49. F. Sherman, "Getting started with yeast," in *Methods Enzymol.* 350 (Elsevier, 2002), pp. 3–41.
50. J. Heisler, L. Elvir, F. Barnouti, E. Charles, T. D. Wolkow, and R. Pyati, "Morphological effects of natural products on schizosaccharomyces pombe measured by imaging flow cytometry," Nat. Prod. Bioprospect. **4**(1), 27–35 (2014).
51. J. Jelsma and D. R. Kreger, "Polymorphism in crystalline (1→ 3)-α-d-glucan from fungal cell-walls," Carbohydr. Res. **71**(1), 51–64 (1979).
52. K. Ogawa, K. Okamura, and A. Sarko, "Molecular and crystal structure of the regenerated form of (1→ 3)-α-D-glucan," Int. J. Biol. Macromol. **3**(1), 31–36 (1981).
53. H. J. Blumenthal and S. Roseman, "Quantitative estimation of chitin in fungi," J. Bacteriol. **74**, 222 (1957).
54. I. Aranaz, M. Mengíbar, R. Harris, I. Paños, B. Miralles, N. Acosta, G. Galed, and Á Heras, "Functional characterization of chitin and chitosan," Curr. Chem. Biol. **3**, 203–230 (2009).
55. D. J. Manners, A. J. Masson, and J. C. Patterson, "The structure of a β-(1→ 3)-D-glucan from yeast cell walls," Biochem. J. **135**(1), 19–30 (1973).
56. D. J. Manners, A. J. Masson, J. C. Patterson, H. Björndal, and B. Lindberg, "The structure of a β-(1→ 6)-D-glucan from yeast cell walls," Biochem. J. **135**(1), 31–36 (1973).
57. P. N. Lipke and R. Ovalle, "Cell wall architecture in yeast: new structure and new challenges," J. Bacteriol. **180**, 3735–3740 (1998).
58. Z. Hromádková, A. Ebringerová, V. Sasinková, J. Šandula, V. Hříbalová, and J. Omelková, "Influence of the drying method on the physical properties and immunomodulatory activity of the particulate (1→ 3)-β-D-glucan from Saccharomyces cerevisiae," Carbohydr. Polym. **51**(1), 9–15 (2003).
59. B. Waszkiewicz-Robak, "Spent brewer's yeast and beta-glucans isolated from them as diet components modifying blood lipid metabolism disturbed by an atherogenic diet," in *Lipid Metabolism* (Intech, 2013).